Electron Transfer Dynamics of *Rhodopseudomonas viridis* Reaction Centers with a Modified Binding Site for the Accessory Bacteriochlorophyll

Thomas Arlt,[‡] Barbara Dohse,[§] Stefan Schmidt,[‡] Josef Wachtveitl,[‡] Evi Laussermair,[||] Wolfgang Zinth,*[,‡] and Dieter Oesterhelt[§]

Institut für Medizinische Optik, Ludwig-Maximilians-Universität, Barbarastrasse 16, 80797 München, Germany, Max-Planck-Institut für Biochemie, Am Klopferspitz 18a, 82152 Martinsried, Germany, and Max-Planck-Institut für Biophysik, Abteilung Molekulare Membranbiologie, 60528 Frankfurt a. M., Germany

Received January 25, 1996; Revised Manuscript Received May 6, 1996[⊗]

ABSTRACT: Femtosecond spectroscopy in combination with site-directed mutagenesis was used to study the influence of histidine L153 in primary electron transfer in the reaction center of *Rhodopseudomonas viridis*. Histidine was replaced by cysteine, glutamate, or leucine. The exchange to cysteine did not lead to significant changes in the primary reaction dynamics. In the case of the glutamate mutation, the decay of the excited electronic level of the special pair P* is slowed by a factor of 3. The exchange to leucine caused the incorporation of a bacteriopheophytin *b* instead of a bacteriochlorophyll *b* molecule at the B_A site. As a consequence of this chromophore exchange, the energy level of the electron transfer state $P^+B_A^-$ is lowered to such an extent that repopulation from the next electron transfer intermediate state $P^+H_A^-$ takes place, resulting in a long-lasting $P^+B_A^-$ population. The observed differences in time constants are discussed in the scope of nonadiabatic electron transfer theory considering the influence of the amino acids at position L153 and the chromophore exchange on the energy level of the intermediate state $P^+B_A^-$. The results show that the high efficiency of primary electron transfer is reduced substantially, if the energy level of $P^+B_A^-$ is lowered or raised by several hundred wavenumbers.

The primary photochemical event during photosynthesis of bacteriochlorophyll-containing organisms is a light-induced charge separation within a transmembrane protein complex called the reaction center (RC).[1] In purple bacteria, the protein complex contains three protein subunits referred to as L, M, and H, according to their respective mobilities in SDS−polyacrylamide gels. Associated with the L and M subunits are the cofactors, consisting of four bacteriochlorophylls (BChl), two bacteriopheophytins (BPhe), one atom of non-heme ferrous iron, and two quinones. Most investigations dealing with purple bacterial photosynthesis were made on the RC of *Rhodobacter sphaeroides*, *Rhodobacter capsulatus*, and *Rhodopseudomonas viridis*, respectively. While *Rb. sphaeroides* and *Rb. capsulatus* contain BChl-*a* and BPhe-*a* as tetrapyrroles, in *Rps. viridis*, BChl-*b* and BPhe-*b* are incorporated. The cofactors are arranged in two branches with an approximate C_2 symmetry called the A and B branch, respectively [for details of the crystal structure, see Ermler et al. (1994)].

The dynamics of the light-induced electron transfer steps have been investigated by time-resolved spectroscopy over the last decade [for an overview, see Deisenhofer and Norris (1993)]. Optical excitation leads to the transfer of an electron away from a pair of strongly coupled bacteriochlorophyll molecules, the so-called special pair P, in about 3 ps. With the same time constant, the arrival of the electron at the bacteriopheophytin H_A on the A branch is observed. The role of the accessory BChl, situated between P and H_A, requires further considerations. Two possibilities for the initial electron transfer exist.

(i) If the free energy *G* of the intermediate state $P^+B_A^-$ lies high above the energy of P*, a superexchange via B_A without a real population of $P^+B_A^-$ would facilitate the rapid initial transfer.

(ii) If the free energy of $P^+B_A^-$ is below or close to that of P*, the two-step mechanism via a real intermediate state $P^+B_A^-$ should be preferentially used.

In the initial femtosecond experiments, the possible intermediate $P^+B_A^-$ was not detected spectroscopically (Martin et al., 1986). These data favored strongly the superexchange mechanism of electron transfer. However, the experimental limits of Martin et al. (1986) allow a two-step process, if the electron transfer from $P^+B_A^-$ to $P^+H_A^-$ is faster than the decay of P* by a factor of about 3 (Marcus et al., 1987). Supporting the stepwise electron transfer model, later experiments on native RCs (Holzapfel et al., 1989; Dressler et al., 1991) have revealed a small absorption change related to a weak and short-lived population of the bacteriochlorophyll anion state B_A^-. The existence of $P^+B_A^-$ as a real intermediate state between P* and $P^+H_A^-$ was strongly supported by recent experiments on isolated RCs (Arlt et al., 1993), membrane-bound RCs (Beekmann et al., 1995), and RCs with exchanged pheophytins (Schmidt et al., 1994, 1995; Huber et al. 1995). These experiments result in the

* To whom correspondence should be addressed. Telephone: 0049/89/12406302. Fax: 0049/89/12406301.
[‡] Ludwig-Maximilians Universität.
[§] Max-Planck-Institut für Biochemie.
[||] Max-Planck-Institut für Biophysik.
[⊗] Abstract published in *Advance ACS Abstracts,* June 15, 1996.
[1] Abbreviations: BChl, bacteriochlorophyll; Chl, chlorophyll; BPhe, bacteriopheophytin; *Rb*, *Rhodobacter*; *Rps*, *Rhodopseudomonas*; RC(s), reaction center(s); LHC, light-harvesting complexes; ET, electron transfer; P, primary donor; $B_{A,B}$, sites of monomeric BChl in the RC; $H_{A,B}$, sites of BPhe-a; $Q_{A,B}$, quinone sites; (indices A and B refer to the position on the active and inactive branch, respectively); HPLC, high-pressure liquid chromatography; LDAO, lauryldimethylamine *N*-oxide; TL, tris-LDAO; DEAE, diethylaminoethyl.

S0006-2960(96)00185-7 CCC: $12.00

following picture of the initial electron transfer (ET) reaction in *Rb. sphaeroides*. From the excited electronic state P*, the electron is transferred within ≈3 ps to the accessory BChl B_A and in a second, faster step with 0.9 ps to the BPhe H_A. The free energy of the intermediate $P^+B_A^-$ is approximately 450 cm^{-1} below that of P* (Schmidt et al., 1994; Bixon et al., 1995). In *Rps. viridis*, the second electron transfer step is faster (0.65 ps) and no distinct value of the free energy of $P^+B_A^-$ was determined until now. The subsequent electron transfer steps are slower. The electron is transfered within ≈200 ps from H_A to the quinone Q_A and in the microsecond range to the quinone Q_B.

At present, investigations of the primary steps in photosynthesis focus more and more on details of the ET such as the energetics of the intermediates, the role of specific amino acids, and the optimization of the energy conversion within the RC (Moser et al., 1992). It has been shown previously that site-directed mutagenesis is a powerful tool to study these questions (Bylina et al., 1988; Gray et al., 1990; Finkele et al., 1990; Williams et al., 1992; Farchaus et al., 1993; Jia et al., 1993; Nagarajan et al., 1993; Heller et al., 1995).

Of particular interest are mutations dealing with the exchange of amino acids that act as ligands to central atoms of various chromophores. For heme proteins, it has been shown that it is possible to replace ligands by a wide range of other small organic ligands (DePillis et al., 1994). In photosynthetic RCs, the bacteriochlorophylls P_A, P_B, B_A, and B_B are ligated via histidine residues through their central Mg atom (Ermler et al., 1994). In *Rps. viridis*, M200H and L173H serve as ligands to the bacteriochlorophylls of the special pair, and L153H and M180H are the ligands to the bacteriochlorophylls B_A and B_B, respectively. For *Rb. sphaeroides*, it is known that the so-called heterodimer consisting of BChl and BPhe is formed when the axial histidine ligands to either of the Mg atoms of the special pair are replaced by leucine (L) or phenylalanine (F) (Bylina & Youvan, 1988). However, very recently, Boxer and coworkers (Goldsmith et al., 1996) have shown that a normal special pair is formed, if these histidine ligands are mutated to glycine (G). It was proposed that in this case water serves as the ligand. In RCs of *Rb. capsulatus*, the H ligands to the monomeric BChls have been mutated to serine (S) and threonine (T) without changing the chromophore bacteriochlorophyll (Bylina et al., 1990). Western blot analysis has shown that no functional RCs are assembled in *Rb. sphaeroides* when the ligand to the bacteriochlorophyll B_A, histidine L153, is replaced by leucine (L) (Wachtveitl, 1992).

While mutant RCs of *Rb. sphaeroides* and *Rb. capsulatus* have been available now for several years, the construction of mutant RCs of *Rps. viridis* has been successful only recently (Laussermair & Oesterhelt, 1992; Dohse et al., 1995).

The rationale to use *Rps. viridis* is based on four arguments. First, the resolution in the structural analysis of the RC obtained is 2.3 Å for *Rps. viridis* but only 2.65 Å in *Rb. sphaeroides* (Ermler et al., 1994), and furthermore, high-resolution structure analysis is possible for mutant RCs of *Rps. viridis*. Second, *Rps. viridis* contains BChl-*b* and BPhe-*b* type chromophores. Third, only *Rps. viridis* RCs exist as a stable complex with a tetraheme cytochrome rereducing its photooxidized special pair, thereby allowing a detailed analysis of the electron transfer reaction between the heme group and the special pair (Dohse et al., 1995). Fourth, in some cases and for unknown reasons, a mutated RC might be expressed stably in *Rps. viridis* but not in *Rb. sphaeroides*. This is the case for a set of mutations discussed in this contribution and concerning the position L153, which in wild type (WT) is a histidine residue forming the fifth ligand to the central Mg atom of the accessory bacteriochlorophyll B_A. Considering the results obtained for the heterodimer (see above), replacement of this amino acid could result in the exchange of bacteriochlorophyll by a bacteriopheophytin and an alteration of energetics and kinetics of the initial steps in photosynthetic charge separation after photoexcitation.

In this paper, we present experiments on RCs in which the ligand histidine L153 was replaced by cysteine (L153HC), glutamate (L153HE), and leucine (L153HL). We report results obtained from femtosecond spectroscopy of the primary reaction dynamics of the mutants and show that the location of the energy level of the intermediate state $P^+B_A^-$ is crucial for the high efficiency of the primary steps of light-induced electron transfer.

MATERIALS AND METHODS

Bacterial Strains and Growth Conditions. Rps. viridis cells (DSM 133) were grown photoheterotrophically in N-medium (Lang & Oesterhelt, 1989). The mutants were cultivated on plates with 20 μg/mL kanamycin and 10 μg/mL tetracycline and grown in liquid culture with only 20 μg/mL kanamycin in N-medium. The mutant strains contain plasmid pRK 404 (Ditta et al., 1985) with the RC genes carrying the appropriate mutation. The mutation introduced was confirmed for all mutants by sequence analysis of the DNA isolated from the cell batch used for isolation of the RC.

Construction of Strains. The construction of a *puf* operon deletion strain and the complementation to site-specific mutants has been described previously (Laussermair & Oesterhelt, 1992). Site-specific mutagenesis was performed following the instruction manual of the Muta-Gene *in vitro* mutagenesis kit (Bio-Rad). The mismatched oligonucleotides were synthesized by the phosphoramidite method on an Applied Biosystems DNA synthesizer (model 381A). The wild type histidine L153 codon CAT is replaced in the mutants by the following base triplets: L153HC, TGT; L153HL, CTG; and L153HE, GAG.

Protein Isolation. Rps. viridis was grown phototrophically in Nalgene bottles completely filled with N-medium containing 20 μg/mL kanamycin. The cells were harvested after 1 week of growth by centrifugation in a Stock centrifuge for 30 min at 4000*g* and washed in 20 mM Tris/HCl (pH 8.0). The yield of cells was typically 30−40 g of wet weight per 25 L. The cell pellet could be frozen in liquid nitrogen and stored at −20 °C. A sample was taken out of each culture, and from these, the DNA was isolated and sequenced. The processing of the cells was only continued in those cases when the sequence of the introduced mutation was reconfirmed. The RC was isolated using a modified method as described for *Rb. sphaeroides* (Farchaus et al., 1993). For protein isolation, the pellet was resuspended in 3 mL/g cells of 20 mM Tris/HCl (pH 8.0) and stirred for 30 min at room temperature in the presence of DNase I. The cells were broken by treatment in a French Pressure cell (Aminco, Lorch, Germany). Chromatophores were isolated as de-

scribed (Farchaus et al., 1993) and suspended in 20 mM Tris/HCl (pH 8). To isolate reaction centers, chromatophore suspensions with an optical density (OD) of 50 at 1020 nm were solubilized by addition of LDAO to a final concentration of 5%. Light-harvesting complexes (LHC) are destroyed at this detergent concentration. The solution was centrifuged for 60 min at 200000*g* and the supernatant dialyzed against 20 mM Tris/HCl (pH 8) and 0.08% LDAO (TL buffer). Reaction centers were then purified on a DEAE ion exchange column. When the column was rinsed with 20 mM Tris/HCl buffer (pH 8) containing 1.2 % LDAO, free pigments from the LHC and contaminating membrane proteins were eluted. Before the reaction center fraction was eluted with 150 mM NaCl in 20 mM Tris/HCl (pH 8), the column was washed with 3 column volumes of TL buffer. Fractions of the eluate were analyzed spectroscopically, and only fractions with a small or absent absorption at 680 nm (indicating contamination by free pigments) were combined and dialyzed against TL buffer. If necessary, reaction center solutions were concentrated by centrifugation in Centricon-30 tubes, frozen in liquid nitrogen, and stored at −20 °C. Prior to any experiment, the material was assayed by SDS gel electrophoresis to check whether the RC isolated contained all four subunits.

Isolation of the DNA. A sample of the cells was resuspended in 100 μL of proteinase K (10 mg/mL) solution, incubated for 30 min at 37 °C, and blended afterward with 30% sodium sarcosinate. The proteins were separated by adding 400 μL of phenol. The phenol was removed from the aqueous phase containing the DNA by extraction with $CHCl_3$, and then the DNA was precipitated with ethanol and redissolved in H_2O.

Sequencing. With the aid of two primers, a 800 bp fragment was amplified from the *puf*L gene of the chromosomal DNA. This product was sequenced by means of the Taq-Dye-Deoxy-Terminator-Cycle-Sequenzing Kit (Applied Biosystems, Germany).

Photoinduced Difference Spectra. Difference spectra were recorded from suspensions of intact cells or solutions of isolated RCs. RC samples were in 20 mM Tris (pH 8) at a redox potential where both high-potential hemes were reduced prior to illumination. Samples with an optical density of 2 at 1020 nm (intact cells) or of 2 at 830 nm (isolated RC) were illuminated with white light from a halogen lamp which passed an RG 610 long-pass filter before entering the samples (5 mW/cm^2). The optical path length was 1 cm. The light beam was dispersed after the sample and measured by diodes in the range from 680 to 990 nm at 10 nm intervals. Due to the intensity of the measuring beam, the photooxidized special pair accumulated in time, thus allowing the difference spectra to be recorded within the 64 ms measuring period.

Electrochemical Redox Titrations. Titrations were carried out with the same setup as used for measuring difference spectra and as described elsewhere (Wachtveitl et al., 1993). Samples were placed in a cuvette with an optical path length of 0.2 mm, equipped with a gold mesh measuring electrode, a platinum wire as a counter electrode, and an Ag/AgCl electrode as reference. Samples of isolated reaction centers with an OD_{830} of 2−3 were kept at voltages between 270 and 600 mV with the help of a potentiostat (EG&G). Spectra were recorded after 1 s of illumination at different potentials. Individual spectra were taken every 10−20 mV.

Femtosecond Spectroscopy. The transient absorption experiments in the sub-picosecond time range were performed at room temperature by a laser-amplifier system based on a CPM dye laser (Schmidt et al., 1993). The basic features of the system are as follows: repetition rate, 50 Hz; excitation wavelength (λ_{exc}), 960 nm; probing pulses in the range between 550 and 1050 nm; and a width of the instrumental response function of 250 fs.

The experiments were performed in general with parallel polarization between pump and probe pulses; the use of perpendicular polarization is noted explicitly. The sample was held in a cuvette with a 1 mm path length and stirred continuously. The concentration of the RC was adjusted to 50 μM. For probing wavelengths in the 830 nm region, a concentration of 25 μM was used. About 15% of the RCs were excited in the irradiated volume. For modeling of the ultrafast reaction dynamics, nonadiabatic electron transfer (ET) theory (Marcus & Sutin, 1985; Bixon et al., 1991) is applied and the reaction is described by a rate equation system (Schmidt et al., 1995). The intermediates I_i and I_j of the ET processes are connected by microscopic rates γ_{ij} (see Figure 5). These microscopic rates γ_{ij} are the elements of a rate matrix. The exponential decay rates determined in the time-resolved experiments correspond to the eigenvalues $k_i = 1/\tau_i$ of the rate matrix. When only a linear reaction scheme without back-reactions applies (as e.g. for ultrafast processes in WT RCs), the observed decay rates k_i are identical with the microscopic forward rates $\gamma_{i(i+1)}$:

$$I_0 \xrightarrow{h\nu} I_1 \xrightarrow[1/\gamma_{12}]{\tau_1} I_2 \xrightarrow[1/\gamma_{23}]{\tau_2} I_3 \xrightarrow[1/\gamma_{34}]{\tau_3} I_4$$

The situation is different, if branching, backward rates or recombination processes are involved (Schmidt et al., 1995). For example, if there are two decay channels for the first intermediate state I_1 with microscopic rates γ_{10} and γ_{12}, the decay rate observed in the experiment (eigenvalue k_1) is given by $k_1 = \gamma_{10} + \gamma_{12}$. In the figures, the experimental data are normalized to the value 1 and displayed as points, squares, or triangles. For the theoretical modeling of the transient absorption data, a sum of exponentials weighted with amplitudes and convoluted with the instrumental response function is used and displayed as a solid line.

RESULTS

Absorption Spectra. The absorption spectra of different samples are presented in Figure 1a. The RCs of mutant L153HC (data not shown) exhibit a WT-like spectrum. In the spectrum of the L153HE mutant, some differences with respect to the WT spectrum are observed in the Q_y(B,H) band (Figure 1a). In this region, the absorption bands of BChl-*b* and BPhe-*b* overlap. The spectrum of the WT RC shows a band with an absorption peak at 830 nm due to the monomeric BChl-*b* molecules and a pronounced shoulder at the short wavelength side assigned to the Q_y transitions of the BPhe-*b* molecules. In L153HE, we find a reduced absorbance of this band and a shift of the peak toward shorter wavelengths by about 6 nm. The L153HL RCs show pronounced characteristic spectral changes at several positions (Figure 1a). The BChl-*b* absorption bands in the Q_x and the Q_y region (at 600 and 830 nm) are weaker and BPhe-*b* contributions are stronger than in the corresponding spectrum of WT RCs. The absorption at shorter wavelengths

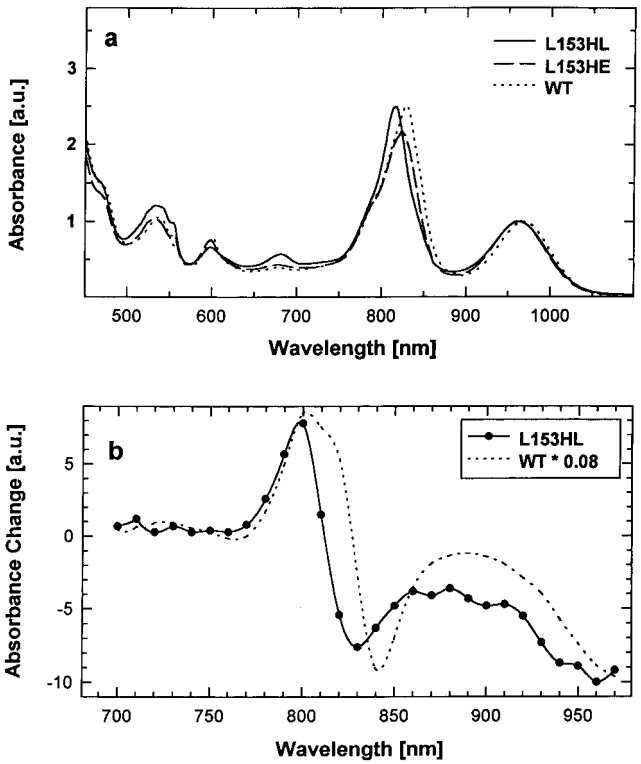

FIGURE 1: (a) Steady state absorption spectra (normalized at 960 nm) of reaction centers of *Rps. viridis* WT (dotted line), mutant L153HE (broken line), and mutant L153HL (solid line). In the mutant L153HL, histidine L153 is replaced by leucine and as a consequence a bacteriopheophytin is incorporated at the B_A site. (b) Light-induced difference spectra of the L153HL mutant (solid line) and of the WT RC (dotted line, reduced scale).

in the Q_y(B,H) band is strongly enhanced in the L153HL RC, shifting the peak of the band to 813 nm. A small absorption band around 680 nm appears as an additional feature mainly in the spectrum of the L153HL RC preparations. This band should be due to a small amount of free or oxidized tetrapyrrole molecules from (partially) denatured RC proteins.

A quantitative determination of the pigment content was performed for WT and all three mutants by extracting the pigments with organic solvents and separating them on a HPLC column. While L153HC and L153HE show the WT ratio of BChl-*b* to Bphe-*b*, the L153HL mutant behaves differently. Quantitative analysis of the eluate shows that, compared to that of WT RCs, the BChl-*b*/BPhe-*b* ratio is reduced by a factor of 1.9 (±0.4) in the L153HL mutant. The uncertainty in the determination of the pigment content is mainly due to the increased amount of free pigment found in this mutant. This result indicates that L153HL RCs contain similar amounts of BChl-*b* and BPhe-*b*.

It can therefore be concluded that the replacement of histidine at the position L153 by leucine leads to the incorporation of a BPhe-*b* instead of a BChl-*b* at the B_A site. Crystallization and X-ray structural analysis of the mutant RCs confirmed that the B_A binding pocket indeed contains a BPhe-*b* molecule (C. R. Lancaster, private communication).

Photoinduced Difference Spectra and Electrochemical Redox Titrations. The photoactivity of the RCs was tested with intact cells and isolated protein by recording P^+-P photobleaching difference spectra. Upon illumination of wild type samples, the main features in the wavelength region between 700 and 1000 nm are bleaching of the P band at 960 nm and the electrochromic shift of the BChl-*b* band from 830 nm to shorter wavelengths (Figure 1b). While the difference spectrum for the L153HC mutant is similar to that of wild type (data not shown), the photoactivity of the two other mutants is clearly reduced. In Figure 1b, the results obtained for the L153HL mutant are compared with the WT data. Only a drastic increase of irradiance (by a factor of 10) and illumination time (by a factor of 15) leads to a P^+-P photobleaching signal in the mutant, which is spectrally similar to WT (Figure 1b), but reduced in amplitude. The photooxidation of P can be seen by the decrease of the signal around 960 nm and the electrochromic shift in the 800−850 nm region, which is found in the mutant at shorter wavelengths ($\Delta\lambda \approx 15$ nm) than in WT RCs. This is another indication that in this mutant the photoactive BChl-*b* is replaced by BPhe-*b* having its absorption band at shorter wavelengths.

The reduced photoactivity directly influences the photosynthetic growth rates of the mutants; the generation time of wild type cells (12 h) is increased to 17 h in the L153HE mutant and to 22 h in the L153HL mutant. This indicates that an additional and/or an accelerated recombination channel is introduced by the mutations. These recombination kinetics occurring on a longer time scale (>1 ns), together with the difference spectra, will be discussed in detail in a forthcoming publication (J. Wachtveitl, unpublished experiments).

The redox midpoint potentials of the primary donor of the various samples are summarized in Table 1. It can be seen that, within the experimental error of ±10 mV, the amino acid change at position L153 has little influence on the P^+/P-midpoint potential. The exception is the L153HE mutant, which has a lower potential by approximately 45 mV.

Femtosecond Spectroscopy. The population of the excited electronic level P* of the special pair can be investigated via its stimulated emission (gain) in the long wavelength region of the special pair Q_y band. Figure 2a shows the detected transient absorption changes of the mutants at 1020 nm. The kinetic components of the mutant RCs are given in Table 1. The mutant L153HE shows a substantially longer monoexponential kinetic component (time constant τ_1) than the WT RC (12 instead of 3.5 ps; Dressler et al., 1991), while the decay times of the mutants L153HC and L153HL are in the range reported for the WT. The monoexponential decay constants can be used as a qualitative estimate for the lifetime of the excited electronic level P*. However, monoexponential fit functions describe the decay of P* insufficiently. As a consequence, a biexponential fit function is used (time constants τ_{1A} and τ_{1B}). The time constants for a biexponential modeling of the P* decay are 3 and 43 and 7 and 40 ps for the L153HL and L153HE mutants, respectively.

In the Q_y(P) band, at 954 nm (Figure 2b), the decay of P* and the recovery of the dimer ground state absorption is observable. In WT and L153HC RCs (data not shown), the bleaching of the Q_y(P) absorption stays constant aside from a small contribution of stimulated emission in the picosecond range. However, in the mutants L153HL and L153HE, a considerable part of the ground state absorption recovers, pointing to a decrease in P^+ concentration. The levels reached after a delay time of 1 ns indicate that the quantum yield of $P^+Q_A^-$ formation of about 97% (Trissl et al., 1990)

Table 1: Decay of the Excited Electronic State P* at 1020 nm and P/P^+-Midpoint Potentials for the Various L153 Mutants and WT RC of *Rps. viridis*

reaction center	monoexponential fit function τ_1 (ps)	biexponential fit function τ_{1A} (ps)	biexponential fit function τ_{1B} (ps)	ratio of the amplitudes $a(\tau_{1A})/a(\tau_{1B})$	P/P^+-midpoint potential (mV)
WT	3.5 ± 0.5	1.8 ± 1	7.4 ± 3	1.4 ± 0.8	520
L153HC	3.8 ± 0.5	2.5 ± 1	10 ± 5	2.6 ± 1.0	522
L153HE	12 ± 3	7 ± 3	40 ± 15	2.0 ± 0.8	475
L153HL	3.5 ± 0.5	3 ± 1	43 ± 20	3.5 ± 1.2	520

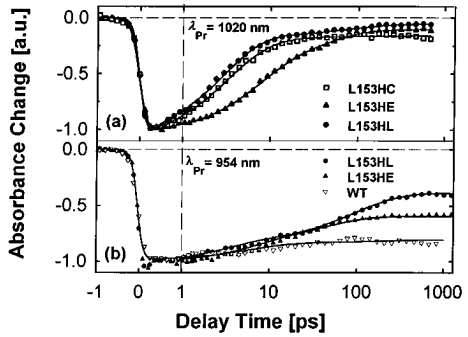

FIGURE 2: Transient absorption data (circles, triangles, and squares) of the different mutants and the WT RC at 1020 nm (a) and 954 nm (b). The solid curves at 1020 nm are calculated by using a biexponential function. The time constants and amplitudes are given in Table 1. At 954 nm (b), the same time constants are used to fit the data of the L153HE mutant and the WT RC. For the L153HL mutant, an additional time constant of 140 ps is required to simulate the data. Note the linear scale for the delay times of <1 ps and the logarithmic scale at later delay times.

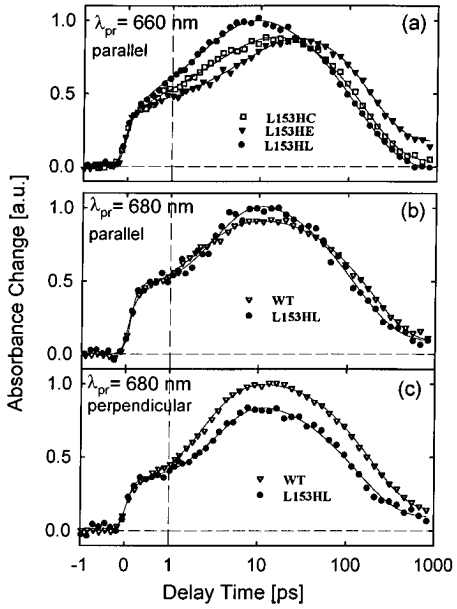

FIGURE 3: Polarization-dependent transient absorption data at 660 and 680 nm for the L153 mutants and the WT RC of *Rps. viridis* (squares, triangles, and points). The solid curves are model functions calculated using the following time constants: WT, 0.65, 1.8, 7.4, and 200 ps; L153HC, 0.65, 2.5, 10, and 160 ps; L153HE, 7, 40, and 170 ps; and L153HL, 1.5, 3, 43, and 140 ps.

in WT RCs is reduced in the mutants to $50 \pm 10\%$ (L153HL) and $75 \pm 10\%$ (L153HE). Since the direct recombination times from the transfer states $P^+H_A^-$ and $P^+Q_A^-$ in wild type RC are in the nanosecond and millisecond time range, respectively (Ogrodnik et al., 1988), this reduced quantum yield must be due to recombination events via early intermediate states modified by the mutation (see below).

For the L153HE mutant, the partial recovery of absorption at 954 nm proceeds with the same time constant obtained from stimulated emission at $\lambda = 1020$ nm ($\tau_1 = 12$ ps). For L153HL, 40% of the absorption recovery occurs with an additional time constant of 140 ± 50 ps.

The decay of the bacteriopheophytin anion population, i.e. the decay of the radical pair state $P^+H_A^-$, can be clearly seen by probing in the spectral range from 600 to 700 nm (Figure 3), where observation of the BChl-*b* and BPhe-*b* anion radicals is possible (Dressler et al., 1991). Figure 3a shows the transient absorption data for the L153 mutants at 660 nm. The strong initial rise of absorption is related to the formation of P*. The absorption increase in the picosecond time range is caused by the formation of the anion radicals absorbing around 660 nm. The subsequent absorption decrease is connected with the decays of states $P^+H_A^-$ and $P^+B_A^-$, respectively (see below). The observed time constants for this process(es) are as follows: $\tau_3 = 160 \pm 30$ ps for L153HC, $\tau_3 = 170 \pm 30$ ps for L153HE, and $\tau_3 = 140 \pm 30$ ps for L153HL; i.e. this reaction is accelerated in the mutants compared to the reaction in the WT RC (200 ps; Dressler et al., 1991) by 15−20%. Dichroic measurements in this spectral region are shown in panels b and c of Figure 3 for the mutant L153HL and WT. The absorption increase caused by the population of the anion radicals is more pronounced for a parallel polarization in the L153HL mutant than in the WT RC (Figure 3b) and the other mutants (Figure 3a). For a perpendicular polarization, the opposite response is observed (Figure 3c). It should be noted, that an adequate simulation of the transient data of WT and L153HL at 660 and 680 nm requires an additional short kinetic component in the 1 ps range. The consequence of this observation will be discussed below.

In Figure 4, we present the results of time-resolved absorption measurements in the spectral range of the Q_y transition of the monomeric bacteriochlorophyll and bacteriopheophytin, respectively. In Dressler et al. (1991), it was shown for the WT RC of *Rps. viridis* that an additional process with a short time constant of $\tau_2 = 0.65$ ps could be detected in the region of the Q_y transition of the monomeric bacteriochlorophyll. This additional signal was assigned to the intermediate $P^+B_A^-$. The weak amplitude of this absorbance change was explained by a small population (about 12%) of the state $P^+B_A^-$ within the sequential ET model (Holzapfel et al., 1989; Dressler et al., 1991). The fast process was seen best at wavelengths where the 3.5 ps process has a vanishing amplitude. In the region of the monomeric BChl B_A, this wavelength is in the vicinity of the isosbestic point of the $PQ_A/P^+Q_A^-$ difference spectrum, which is determined by an electrochromic blue shift of B_A. The exact position of the isosbestic points is expected to be different for mutations influencing the accessory BChl. In the L153HL mutant, the isosbestic point is at much shorter wavelengths ($\Delta\lambda \approx 15$ nm, see Figure 1b) than in WT RCs.

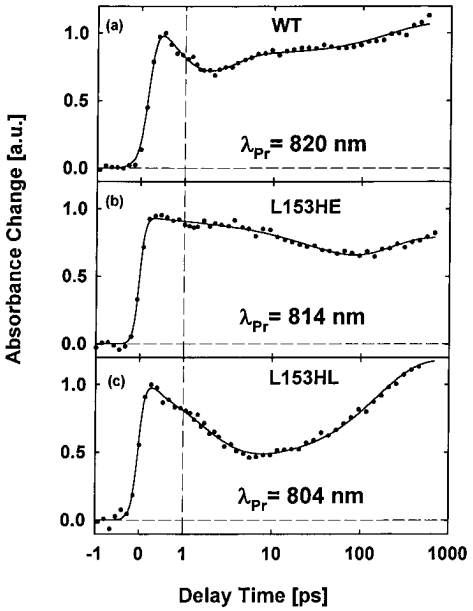

FIGURE 4: Transient absorption changes in the region of the Q_y absorption of the bacteriochlorophylls and bacteriopheophytins: (a) WT, (b) L153HE, and (c) L153HL. Model functions of the data using the same time constants as in Figure 3 are displayed as solid lines.

This change is caused by the replacement of the BChl by a BPhe in the binding pocket B_A. Figure 4 shows the time-resolved data at the positions of the isosbestic points for the L153 mutants and the WT RC. The observed initial absorbance changes (rise of absorbance due to P* formation) are similar in mutants and the WT RC. At longer delay times, differences are found. The L153HL preparation (Figure 4c) shows a strong transient absorption decrease in the 1−10 ps range, which is more pronounced than in the WT RC (Figure 4a). An accurate simulation of these data yields an additional fast time constant of $\tau_2 = 1.5 \pm 0.6$ ps for L153HL (0.65 ± 0.3 ps for the WT RC). In the L153HE mutant, only negligible absorbance differences connected with a fast time constant of ≈1 ps occur. At all investigated wavelengths, we do not find a significant amplitude related to a short 0.65−1.5 ps kinetic component in L153HE.

DISCUSSION

Ligands to the Bacteriochlorophyll B_A. In principle, a number of acidic amino acid side chains [glutamate (E), aspartate (D), glutamine (Q), asparagine (N), cysteine (C), serine (S), threonine (T), histidine (H), methionine (M), or even water] can serve as ligands to the Mg of BChl (Fenna & Matthews, 1975). In photosynthetic reaction centers, the Mg atoms of the bacteriochlorophyll molecules are ligated by histidine residues (Ermler et al., 1994). Bylina and co-workers (Bylina et al., 1990) have shown that serine (S) and threonine (T), in contrast to leucine (L), can ligate the Mg atoms of the primary donor in photosynthetic RCs. The absorption spectra of the L153 mutants of *Rps. viridis* yield similar results; while cysteine (L153HC) and glutamate (L153HE) are able to ligate the Mg atom, the mutation to leucine (L153HL) results in a chromophore exchange. The blue shift and altered oscillator strength of the Q_y(B) band, but not of the Q_y(H) band, points to some perturbations of the electronic structure of the BChl B_A in the L153HE mutant. The state of ionization of the introduced glutamic acid residue at position L153 in the RC is not known. This problem will be discussed in more detail below. In the literature, there are examples where glutamate or an aspartate is also found as a ligand in photosynthetic systems: for the plant light-harvesting chlorophyll *a*/*b*−protein complex it has been shown that in LHC-II three side chain ligands are glutamates (Kühlbrandt et al., 1994). Michel and co-workers (Koepke et al., 1996) have demonstrated very recently that B800 BChl molecules in the light-harvesting complex II from *Rhodospirillum molischianum* exhibit a ligation involving an aspartate side chain.

Biphasic Decay of the Excited State P.* It has been shown in the literature that a multiphasic decay of P* exists in WT RCs of *Rb. sphaeroides* and *Rb. capsulatus* (Du et al., 1992; Hamm et al., 1993; Jia et al., 1993; Ogrodnik et al., 1994). This non-monoexponential decay contains one short dominant component and a number of weaker and longer-lived components. A model which is based on a population of B_B at the "inactive" branch (parking model; Hamm et al., 1993) is not able to explain the nonexponentiality. Since the energy of $G(P^+B_B^-)$ is thought to lie above G(P*) (Parson et al., 1990), the deviations from a monoexponential decay should become smaller at low temperatures. However, the opposite is observed experimentally (Vos et al., 1991; Jia et al., 1993; Nagarajan et al., 1993). The assumption of sample heterogeneity with a distribution of electron transfer parameters is a straightforward way to explain the non-monoexponentiality (Du et al., 1992; Jia et al., 1993). One possibility is a distribution of the free energy of the ET intermediate states. A distribution of the free energy of the state $P^+H_A^-$ with a spread of ≈400 cm^{-1} was introduced by Ogrodnik and co-workers (Ogrodnik et al., 1994) to explain their data on delayed emission and radical pair recombination. Bixon and co-workers used the same distribution for the energy level of the state $P^+B_A^-$ in order to simulate the energetics and heterogeneity of the P* decay of a number of mutated RCs of *Rb. sphaeroides* (Bixon et al., 1995).

The dynamic range of the pump−probe experiments presented here allows a reasonable modeling of the experimental data of *Rps. viridis* by a biexponential fit function (τ_{1A} and τ_{1B} in Table 1). In WT RCs of *Rps. viridis*, the fast component ($\tau_{fast} = \tau_{1A} = 1.8$ ps) is still dominant. However, the contribution is smaller than in *Rb. sphaeroides*; the amplitude ratio amounts to $a_{1A}/a_{1B} \approx 1.4$ for *Rps. viridis* and $a_{1A}/a_{1B} > 2$ for *Rb. sphaeroides*. In all investigated samples of *Rps. viridis*, the slower second component was observed. In the mutants L153HE and L153HL, where the B_A binding pocket was altered significantly, the ratio of the time constants τ_{1B}/τ_{1A} is strongly increased (τ_{1B} in the range of 40−50 ps). This finding is compatible with the idea that a distribution of the energy level $G(P^+B_A^-)$ (Bixon et al., 1995), modulated by the properties of the binding pocket, is responsible for the nonexponential decay characteristics. Since the biexponentiality also occurs in most other reaction centers, it seems that a distribution of ET parameters is a general property of bacterial RCs. In order to simplify the further discussion, we will only use the time constant from the monoexponential fits of the data (τ_1) as a qualitative measure of the P* decay.

First ET Step in the Mutants in the Scope of Nonadiabatic Theory. In this section, we discuss the data in the frame of nonadiabatic electron transfer theory (Marcus & Sutin, 1985; Bixon et al., 1991). Our considerations are based on the

monoexponential decay times τ_1 in order to describe the observed different absorbance changes in the mutants. If the faster decay components of the biexponential fit functions are considered, qualitatively, the same results are obtained.

In the high-temperature limit, the transfer rate constant depends on the free energy difference ΔG of the reactant and product state and the temperature T according to the expression

$$k = \frac{2\pi}{\hbar}|V|^2\mathrm{FC} = \frac{2\pi}{\hbar}\frac{|V|^2}{\sqrt{4\pi\lambda k_\mathrm{B}T}}\exp\left[-\frac{(\Delta G+\lambda)^2}{4\lambda k_\mathrm{B}T}\right] \quad (1)$$

where FC is the Franck−Condon factor, λ the reorganization energy, and V the electronic coupling matrix element (Marcus & Sutin, 1985). According to eq 1, the logarithm of the rate plotted as a function of the free energy difference ΔG is a parabola (Marcus parabola); the rate k reaches a maximum for $-\Delta G = \lambda$ and decreases with increasing and decreasing values of ΔG. The range where $-\Delta G < \lambda$ is called the activated or normal region and the range where $-\Delta G > \lambda$ the inverted region.

In the following discussion, we explain the influence of the mutations on the primary reaction by changes in ΔG. We assume that the effects induced by the mutations originate from the molecular properties of the exchanged amino acids and chromophores. Structural disorder due to the mutations is assumed to be a secondary effect, since no large differences between mutant and WT RCs are observed in X-ray structure analysis (C. R. Lancaster, private communication).

The changes $\Delta\Delta G$ in the free energy of the first ET step can be estimated for several situations. If the energy level of P, the absorbance spectrum of the Q_y(P) band, and the chromophores are not affected by the mutation, the standard free energy change $\Delta\Delta G$ of a P^+-containing intermediate state (P^+I^-) can be estimated by the change of the P/P^+-midpoint redox potential $\Delta U_{P/P+}$:

$$\Delta\Delta G(\mathrm{P^*{-}P^+I^-}) = \Delta G(\mathrm{P^*{-}P^+I^-})_\mathrm{WT} - \Delta G(\mathrm{P^*{-}P^+I^-})_\mathrm{Mut} \approx \Delta U_{P/P+} \quad (2)$$

Here, a decrease of $U_{P/P+}$ with respect to WT RCs ($\Delta U_{P/P+} > 0$) corresponds to a decreased energy level of the intermediate state P^+I^- in the mutant and a more negative free energy difference $\Delta G(\mathrm{P^*{-}P^+I^-})_\mathrm{Mut}$. If in addition a chromophore of an intermediate state, for example B_A, is changed by the modification, the free energy change is given by

$$\Delta\Delta G(\mathrm{P^*{-}P^+I^-}) \approx \Delta U_{P/P+} + \Delta U_\mathrm{Chrom} \quad (3)$$

ΔU_Chrom is the *in vitro* difference of the midpoint redox potential of the exchanged chromophores. Since there is no other possibility to estimate the *in vivo* difference of the midpoint potential, one has to use the *in vitro* value, e.g. in dimethylformamide. In this context, it must be noted that the value of a redox potential depends strongly on the solvent used. However, the difference of the midpoint potentials of BPhe and BChl, which is used for the estimate in eq 3, is less solvent-dependent (Scheer, 1991).

In this paper, we investigate RCs mutated at position L153; i.e. close to B_A. As a consequence, the main differences should be induced for the intermediate state $P^+B_A^-$. Equations 2 and 3 will be used to estimate the energetics of the radical pair state $P^+B_A^-$.

In the L153HC mutant, no pronounced differences are observed with respect to the WT. In addition, this mutant exhibits an unchanged midpoint potential P/P^+ (see Table 1). Since cysteine can also provide an electron to act as a ligand for the central Mg atom of the BChl (see above), this behavior could be expected. Depending on the interaction of the sulfur d orbitals in cysteine with the central Mg atom, the energy level of $P^+B_A^-$ could be weakly raised compared to that of WT. This may lead to the observed weak slowing of the P* decay times (3.8 instead of 3.5 ps).

In the L153HE mutant, a slower P* decay time of 12 ps and a reduced quantum yield of about 75% are observed. If we use eq 1 with a constant coupling V, $\Delta G = G(\mathrm{P^*}) - G(\mathrm{P^+B_A^-})$, and assume that WT RCs are in the activated region, the slowing of the P* decay points to an increase of the energy level of $P^+B_A^-$. On the other hand, P/P^+-redox potential is decreased by about 45 mV in this mutant, and eq 2 would lead to a decrease in $\Delta\Delta G$. A possible explanation of this contradiction can be obtained by using eq 3 and considering a change in redox potential of BChl by the presence of glutamate. If glutamate is ionized, a negative charge is introduced at position L153 (close to B_A) and a strong rise in the energy level of $P^+B_A^-$ will occur, which cannot be detected by the P/P^+-midpoint potential $\Delta U_{P/P+}$. A slower P* decay connected with the introduction of a negative aspartic acid residue near B_A was also observed in the M203GD mutant of *Rb. sphaeroides* (Williams et al., 1992). In this mutant, the change in the P/P^+-midpoint potential also did not correlate with the observed slower time constant. In addition, comparing the data on the L153HE mutant with L153HC RCs [changed Q_y(B) absorption band and slower P* decay in L153HE], we can conclude that in L153HE additional effects occur. One possibility could be that the slowing is due to the introduction of a negatively charged glutamate in L153HE as proposed above. However, it must be noted that (i) to date there is no direct experimental determination of the state of ionization of the glutamic acid residue at position L153 and (ii) the observed decay time constant could be caused by small changes in distance (below X-ray resolution) leading to an altered coupling V in eq 1.

A consequence of the slower first electron transfer rate in the L153HE mutant is that in the two-step model the maximum population of $P^+B_A^-$ under the condition of an unchanged depopulation of $P^+B_A^-$ is very low (5% at best). Indeed, no short component connected with a transient population of $P^+B_A^-$ could be detected in the absorbance measurements of this mutant (see Figure 4b). In addition, a direct electron transfer to H_A (superexchange mechanism) may also become important relative to the two-step process, if the energy level of $P^+B_A^-$ is raised in the mutant L153HE.

The slowing of the P* decay in L153HE allows one to explain the observed change in quantum yield. Using the reaction model of Figure 5 with a recombination rate γ_{10} from P* to ground state P, the fraction of RC which recombines from P* is $\gamma_{10}\tau_1$. The large recombination yield of about 25 ± 10% in the L153HE mutant can be explained by a direct ground state recombination rate γ_{10} of $1/\gamma_{10} \approx 1/(50\ \mathrm{ps} - 100\ \mathrm{ps})$. The recombination may occur from the initially excited state P* or from a possible intradimer charge transfer state (Kirmaier & Holten, 1993). A reduced

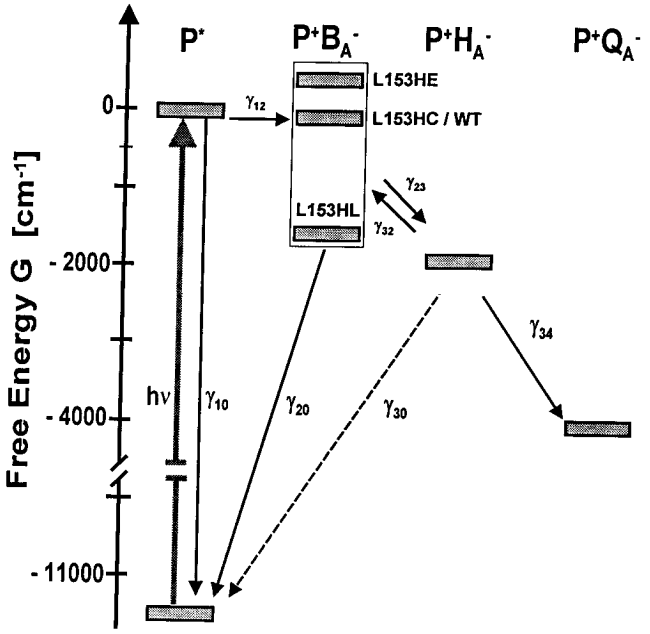

FIGURE 5: Schematic reaction model of the primary electron transfer of the RC of *Rps. viridis*.

quantum yield connected with a slow P* decay was also observed in other mutants of *Rps. viridis* where tyrosine M208 was replaced by phenylalanine (T. Arlt, unpublished experiments). In these M208 mutants, a rate constant γ_{10} in the same range can be estimated. This finding differs from published results on RCs of *Rb. sphaeroides* and *Rb. capsulatus*, where in the corresponding M210 mutants no reduced quantum yield was observed (Nagarajan et al., 1990; Jia et al., 1993). These differences may result from the reduced rate γ_{10} (1/170 ps, 1/200 ps) reported for RCs of *Rb. capsulatus and Rb. sphaeroides*, respectively (Vos et al., 1992; Nagarajan et al., 1993).

In the L153HL mutant, the leucine residue is not able to act as a fifth ligand to the Mg of BChl-*b*, and as a consequence, BPhe-*b* is inserted into the binding site. This change should drastically influence the energetics of the radical pair state $P^+B_A^-$, leading to a state we call $P^+\Phi^-$. BPhe-*b* in dimethylformamide has a substantially less negative one-electron reduction potential (−0.5 V) than BChl-*b* (−0.7 V) (Scheer, 1991). According to eq 3, this corresponds to an energy difference $\Delta\Delta G = \Delta G(P^+B_A^-) - \Delta G(P^+\Phi^-) \approx 1600\ cm^{-1}$. Surprisingly, the time constants τ_1 observed in stimulated emission measurements of the L153HL mutant are the same as in wild type. A drastic decrease of ΔG and a nearly unchanged time constant τ_1 can only be explained by the assumption that $G(P^+B_A^-)$ in WT is situated in the activated region of the Marcus parabola and the corresponding level $G(P^+\Phi^-)$ of the mutant in the inverted region. As a consequence, WT RCs of *Rps. viridis* cannot be situated at the peak of the Marcus parabola. This finding agrees with data on RCs of *Rps. viridis* mutated at position L168; the mutant L168HF shows a faster P* decay of 1.1 ps (monoexponential fit) (Zinth et al., 1995). This substantial acceleration of the decay cannot only be due to an altered coupling (structural changes). For an estimate, we assume a reorganization energy $\lambda \approx 800\ cm^{-1}$ (Bixon et al., 1995) and an unchanged coupling in eq 1. To account for the acceleration by a factor of 3 in L168HF, the position of WT RCs of *Rps. viridis* at the Marcus parabola has to be about 800 cm^{-1} away from the point of fastest ET ($-\Delta G = \lambda$). However, this would imply thermal activation of the first ET step (eq 1), which is not observed in low-temperature experiments (Fleming et al., 1989). This contradiction cannot be solved at present, but it may point to changes in the reaction mechanism or the structure upon cooling.

If a one-step ET from P* to $P^+H_A^-$ (Kirmaier & Holten, 1993) with $P^+B_A^-$ as a virtual and high-lying superexchange "intermediate" is assumed for the ET at room temperature, one is not able to explain why nearly the same P* decay constants are observed in the L153HL mutant and WT. In the superexchange model (Michel-Beyerle et al., 1988) via a high-lying $P^+B_A^-$, one would expect that the stepwise ET becomes important in the L153HL mutant, when the exchange of the chromophore BChl by BPhe brings $G(P^+B_A^-)$ down by 1600 cm^{-1}. As a consequence, an accelerated P* decay should be observed in the L153HL mutant.

ET from the Bacteriopheophytin to the Quinone. All mutants with exchanged histidine L153 investigated in this paper display decreased time constants τ_3 for the decay of $P^+H_A^-$ (detected around 660 nm). While in the WT RC the observed decay of $P^+H_A^-$ is due to the ET to the quinone Q_A, other reaction channels seem to contribute to the $P^+H_A^-$ decay in the mutant L153HL. In this mutant, the time constant $\tau_3 = 140 \pm 30$ ps is required to model the data not only at 660 nm (decay of $P^+H_A^-$) but also at 954 nm (decay of P^+); i.e. the 140 ps component is also related with the decreased reaction yield. This observation indicates that in this case the 140 ps component is an eigenvalue of the corresponding rate equation system (see below) dominated by two different microscopic rates (γ_{20} and γ_{34}; see Figure 5). In other words, the low-lying state $P^+\Phi^-$ opens an additional recombination channel. This explanation is not valid for the data on the other two mutants. The weaker decreases of the time constant from 200 ± 30 ps (WT) to 160 ± 30 ps and 170 ± 30 ps in the L153HC and L153HE mutants, respectively, point to minor long range changes induced by the mutation which cannot be addressed in detail.

The State $P^+\Phi^-$ *in the Mutated RC L153HL.* A number of experimental observations are directly related to the state $P^+\Phi^-$. This state should be visible after the initial ET step and, due to its low free energy, be in equilibrium with $P^+H_A^-$. Indeed, the dichroic measurements at 680 nm (Figure 3b,c) show that in the 10−100 ps time range RCs of WT and L153HL behave differently; if we assume that the orientation of BPhe in the B_A-binding pocket in L153HL is the same as for a BChl molecule in WT [angle of the Q_y transition dipole moment of 26° relative to the dipole of P (Arlt et al., 1993)], the stronger absorbance change for parallel polarization in the mutant (Figure 3b) points to a long-lasting $P^+\Phi^-$ population. Comparing the data of WT and the L153HL mutant at 680 nm, one estimates a long-lasting $P^+\Phi^-$ population of about 30%. In agreement with the redox measurements and eq 3, this finding indicates that the energy level of $P^+\Phi^-$ is close to that of $P^+H_A^-$.

The reaction model of Figure 5 and a corresponding rate equation system can be used to find a consistent combination of microscopic rates and free energy differences which can reproduce the experimental parameters (time constants τ_i and quantum yield) of the L153HL mutant. We use the intermediate states I_1 (P*), I_2 ($P^+\Phi^-$), I_3 ($P^+H_A^-$), and I_4 ($P^+Q_A^-$) coupled by microscopic rates γ_{ij} for the transition from I_i to I_j. These microscopic rates are the elements of a

rate matrix. The observed decay rates $k_i = 1/\tau_i$ with $1/\tau_1 = 1/3.5$ ps, $1/\tau_2 = 1/1.5$ ps, $1/\tau_3 = 140$ ps, and $1/\tau_4 = 1/\infty$ ps are the eigenvalues of the rate matrix. The procedure is decribed in detail in Schmidt et al. (1995), where it was used to explain the data of RCs of *Rb. sphaeroides* with exchanged bacteriopheophytins.

The measured decay rates k_i and the quantum yield of 50% in the L153HL mutant can be reproduced by the following parameters (see Figure 5): recombination rates, $\gamma_{10} = 1/100$ ps, $\gamma_{20} = 1/120$ ps; forward rates, $\gamma_{12} = 1/3.2$ ps, $\gamma_{23} = 1/2.5$ ps, $\gamma_{34} = 1/160$ ps; and backward rate, $\gamma_{32} = \gamma_{23} \exp[-(\Delta G_2 - \Delta G_3)/k_B T]$ with $\Delta G_2 - \Delta G_3 = \Delta G(P^+\Phi^-) - \Delta G(P^+H_A^-) = 100 \pm 100$ cm^{-1}.

Backward rates other than γ_{32} can be neglected on the observed time scale because of the large energy differences between the related intermediate states. In the simulation, $\gamma_{10} = 1/100$ ps was taken as a fixed value, since the recombination yield in other mutants of *Rps. viridis* (e.g. M208YF and L153HE) requires a value in this range (see above). If one of the other values deviates by more than 20%, the observed time constants and the quantum yield cannot be reproduced simultaneously. The slowing of the second ET step from $P^+\Phi^-$ to $P^+H_A^-$ ($\gamma_{23} = 1/2.3$ ps in L153HL instead of $\gamma_{23} = k_2 = 1/0.65$ ps in WT) seems to be reasonable, taking the reduced energy difference ΔG between the two intermediate states into account. A small difference in the free energy ($\Delta G_2 - \Delta G_3 = 100 \pm 100$ cm^{-1}) is compatible with the fact that the same BPhe chromophore is present in both binding pockets B_A and H_A. Since it is unlikely that the observed recombination yield of 50% in L135HL is only due to a recombination channel from P* to P (as seen in the L135HE mutant), we have to introduce the additional recombination channel $P^+\Phi^- \rightarrow P\Phi$ with the rate γ_{20}. A time constant of 120 ps for this direct ground state recombination ($\gamma_{20} = 1/120$ ps) calculated above seems to be very fast in view of a value of 500−1000 ps estimated for the recombination from the corresponding intermediate $P^+B_A^-$ in *Rb. sphaeroides* (Schmidt et al., 1994; Bixon et al., 1995). However, it should be noted that this recombination may strongly depend on the energy level of $P^+B_A^-$ ($P^+\Phi^-$) and the energy difference relative to the ground state. Therefore, changes relative to *Rb. sphaeroides* WT are not surprising. If the direct ground state recombination rate $P^+B_A^- \rightarrow PB_A$ takes place in the inverted region (Moser et al., 1992), a decrease of $G(P^+B_A^-)$ should result in an increase of the recombination rate as is observed. In any case, independent of the other parameters of the L153HL mutant, γ_{20} must be large in order to account for the reduced quantum yield of about 50%. A drastically reduced quantum yield was also observed in other RCs where substantially different chromophores were in the different binding pockets of the electron acceptors: e.g. zinc-reconstituted RCs (Kirmaier et al., 1986), RCs with a BChl in the H_A binding pocket (Kirmaier et al., 1991), and RCs with plant pheophytins in the H_A binding pocket (Schmidt et al., 1994). The energy levels of the various intermediates are obviously optimized for effective charge separation.

The presented data allow a rough estimate of the free energy difference $\Delta G(P^+B_A^-)$ of WT RCs; if we assume an energy difference $\Delta G(P^+H_A^-)$ in WT RCs of *Rps. viridis* similar to that in *Rb. sphaeroides* (−2000 to −1600 cm^{-1}; Ogrodnik et al., 1990), an energy difference $\Delta G(P^+\Phi^-)$ close to that of $\Delta G(P^+H_A^-)$ in the L153HL mutant, and a decrease of $\Delta G(P^+B_A^-)$ of 1600 cm^{-1} induced by the BChl replacement in the mutant, we obtain an energy level of $G(P^+B_A^-)$ close to $G(P^*)$ in the WT RC within a few hundred wavenumbers.

CONCLUSION

Experiments on mutant RCs of *Rps. viridis*, where histidine L153 was replaced by cysteine, glutamate, and leucine and where in the latter case BPhe-*b* was introduced instead of BChl-*b* at position B_A, give interesting information on the optimization of primary photosynthesis. The data show that the free energy of the first intermediate $P^+B_A^-$ is of major importance. If the free energy of $P^+B_A^-$ is raised relative to that of wild type RC (as likely, if a negative charge is introduced in the mutant L153HE), the quantum efficiency is lowered considerably. On the other hand, a large energy gap between P* and $P^+B_A^-$ and a small energy gap between $P^+B_A^-$ and $P^+H_A^-$ (as realized in the mutant L153HL) causes a long-lasting $P^+B_A^-$ population and loss in quantum efficiency due to recombination via $P^+B_A^-$; i.e. optimization of RCs requires an energy level of $P^+B_A^-$ which is situated between these two cases. Recombination from and via $P^+B_A^-$ in WT RCs is prevented by the fast reaction (0.65 ps) from $P^+B_A^-$ to $P^+H_A^-$. In addition, the repopulation of $P^+B_A^-$ from $P^+H_A^-$ in WT RCs is negligible because of the large energy difference between these states.

ACKNOWLEDGMENT

We thank Prof. H. Scheer for implementation of the HPLC analysis.

REFERENCES

Arlt, T., Schmidt, S., Kaiser, W., Lauterwasser, C., Meyer, M., Scheer, H., & Zinth, W. (1993) *Proc. Natl. Acad. Sci. U.S.A. 90*, 11757−11761.

Beekmann, L. M. P., Jones, M. R., van Stokkum, I. H. M., & Van Grondelle, R. (1995) in *Photosynthesis: from Light to Biospere* (Mathis, P., Ed.) Vol. I, pp 495−498, Kluwer Academic Publishers, Dordrecht, The Netherlands.

Bixon, M., Jortner, J., & Michel-Beyerle, M. E. (1991) *Biochim. Biophys. Acta 1056*, 301−315.

Bixon, M., Jortner, J., & Michel-Beyerle, M. E. (1995) *Chem. Phys. 197*, 389−404.

Bylina, E. J., & Youvan, D. C. (1988) *Proc. Natl. Acad. Sci. U.S.A. 85*, 7226−7230.

Bylina, E. J., Kolaczowski, S. V., Norris, S. V., & Youvan, D. C. (1990) *Biochemistry 29*, 6203−6210.

Deisenhofer, J., & Norris, J. R., Eds. (1993) *The Photosynthetic Reaction Center*, Academic Press, Inc., San Diego.

DePillis, G. D., Decatur, S. M., Barrick, D., & Boxer, S. G. (1994) *J. Am. Chem. Soc. 116*, 6981−6982.

Ditta, G., Schmidhauser, T., Yakobson, E., Lu, P., Liang, X. W., Finlay, D. R., Guiney, D., & Helsinki, D. R. (1985) *Plasmid 13*, 149−153.

Dohse, B., Mathis, P., Wachtveitl, J., Laussermair, E., Iwata, S., Michel, H., & Oesterhelt, D. (1995) *Biochemistry 34*, 11335−11343.

Dressler, K., Umlauf, E., Schmidt, S., Hamm, P., Zinth, W., Buchanan, S., & Michel, H. (1991) *Chem. Phys. Lett. 183*, 270−276.

Du, M., Rosenthal, S. J., Xie, X., DiMagno, T. J., Schmidt, M., Hanson, D. K., Schiffer, M., Norris, J. R., & Fleming, G. R. (1992) *Proc. Natl. Acad. Sci. U.S.A. 89*, 8517−8521.

Ermler, U., Fritsch, G., Buchanan, S., & Michel, H. (1994) *Structure 2*, 925−936.

Farchaus, J. W., Wachtveitl, J., Mathis, P., & Oesterhelt, D. (1993) *Biochemistry 32*, 10885−10893.

Fenna, R. E., & Matthews, B. W. (1975) *Nature 258*, 573−577.

Finkele, U., Lauterwasser, C., Zinth, W., Gray, K. A., & Oesterhelt, D. (1990) *Biochemistry 29*, 8517−8521.
Fleming, G. R., Martin, J. L., & Breton, J. (1989) *Nature 333*, 190−192.
Goldsmith, J. O., King, B., & Boxer, S. G. (1996) *Biochemistry 35*, 2421−2428.
Gray, K. A., Farchaus, J. W., Wachtveitl, J., Breton, J., & Oesterhelt, D. (1990) *EMBO J. 7*, 1061−1070.
Hamm, P., Gray, K. A., Oesterhelt, D., Feick, R., Scheer, H., & Zinth, W. (1993) *Biochim. Biophys. Acta 1142*, 99−105.
Heller, B. A., Holten, D., & Kirmaier, C. (1995) *Science 269*, 940−945.
Holzapfel, W., Finkele, U., Kaiser, W., Oesterhelt, D., Scheer, H., Stilz, H. U., & Zinth, W. (1989) *Chem. Phys. Lett. 160*, 1−7.
Huber, H., Meyer, M., Nägele, T., Hartl, I., Scheer, H., Zinth, W., & Wachtveitl, J. (1995) *Chem. Phys. 197*, 297−306.
Jia, Y., DiMagno, T. J., Chan, C. K., Wang, Z., Du, M., Hanson, D. K., Schiffer, M., Norris, J. R., Fleming, G. R., & Popov, M. S. (1993) *J. Phys. Chem. 97*, 13180−13191.
Kirmaier, C., & Holten, D. (1993) in *The Photosynthetic Reaction Center* (Deisenhofer, J., & Norris, J. R., Eds.) Vol. II, pp 49−67, Academic Press, Inc., San Diego.
Kirmaier, C., Holten, D., Debus, R. J., Feher, G., & Okamura, M. Y. (1986) *Proc. Natl. Acad. Sci. U.S.A. 83*, 6407−6411.
Kirmaier, C., Gaul, D., DeBey, R., Holten, D., & Schenck C. G. (1991) *Science 251*, 922−926.
Koepke, J., Xiche, H., Muenke, C., Schulten, K., & Michel, H. (1996) *Structure* (in press).
Kühlbrandt, W., Wang, D. N., & Fujiyoshi, Y. (1994) *Nature 367*, 614−621.
Lang, F. S., & Oesterhelt, D. (1989) *J. Bacteriol. 171*, 2827−2834.
Laussermair, E., & Oesterhelt, D. (1992) *EMBO J. 11*, 777−783.
Marcus, R. A. (1987) *Chem. Phys. Lett. 133*, 471−477.
Marcus, R. A., & Sutin, N. (1985) *Biochim. Biophys. Acta 811*, 265−322.
Martin, J.-L., Breton, J., Hoff, A. J., Migus, A., & Antonetti, A. (1986) *Proc. Natl. Acad. Sci. U.S.A. 83*, 957−961.
Michel-Beyerle, M. E., Plato, M., Deisenhofer, J., Michel, H., Bixon, H., & Jortner, J. (1988) *Biochim. Biophys. Acta 932*, 52−70.
Moser, C. C., Keske, J. M., Warncke, K., Farid, R. S., & Dutton, P. L. (1992) *Nature 355*, 796−802.
Nagarajan, V., Parson, W. W., Gaul, D., & Schenck, C. C. (1990) *Proc. Natl. Acad. Sci. U.S.A. 87*, 7888−7892.
Nagarajan, V., Parson, W. W., Davis, D., & Schenck, C. C. (1993) *Biochemistry 32*, 12324−12336.
Ogrodnik, A. (1990) *Biochim. Biophys. Acta 1020*, 65−71.
Ogrodnik, A., Volk, M., & Michel-Beyerle, M. E. (1988) in *The photosynthetic bacterial reaction center. Structure, spectroscopy and dynamics* (Breton, J., & Vermeglio, A., Eds.) pp 177−194, Plenum Press, New York.
Ogrodnik, A., Keupp, W., Volk, M., Aumeier, G., & Michel-Beyerle, M. E. (1994) *J. Phys. Chem. 98*, 3432−3439.
Parson, W. W., Nagarajan, V., Gaul, D., Schenck, C. C., Chu, Z.-T., & Warshel, A. (1990) in *Reaction centers of photosynthetic bacteria* (Michel-Beyerle, M. W. Ed.) Springer Series in Biophysics 6, pp 239−249, Springer-Verlag, Berlin.
Scheer, H., Ed. (1991) *The Chlorophylls*, CRC Press, Boca Raton, FL.
Schmidt, S., Arlt, T., Hamm, P., Lauterwasser, C., Finkele, U., Drews, G., & Zinth, W. (1993) *Biochim. Biophys. Acta 1144*, 385−390.
Schmidt, S., Arlt, T., Hamm, P., Huber, H., Nägele, T., Wachtveitl, J., Meyer, M., Scheer, H., & Zinth, W. (1994) *Chem. Phys. Lett. 223*, 116−120.
Schmidt, S., Arlt, T., Hamm, P., Huber, H., Nägele, T., Wachtveitl, J., Zinth, W., Meyer, M., & Scheer, H. (1995) *Spectrochim. Acta 51A*, 1565−1578.
Trissl, H. W., Breton, J., Deprez, J., Dobek, A., & Leibl, W. (1990) *Biochim. Biophys. Acta 1015*, 322−333.
Vos, M. H., Lambry, J.-C., Robles, S. J., Youvan, D. C., Breton, J., & Martin, J.-L. (1991) *Proc. Natl. Acad. Sci. U.S.A. 88*, 8885−8889.
Vos, M. H., Lambry, J.-C., Robles, S. J., Youvan, D. C., Breton, J., & Martin J.-L. (1992) *Proc. Natl. Acad. Sci. U.S.A. 89*, 613−617.
Wachtveitl, J. (1992) Electron Transfer Reactions in Modified Photosynthetic Reaction Centers of Rb. Sphaeroides, Ph.D. Thesis, University of Munich, Munich, Germany.
Wachtveitl, J., Farchaus, J. W., Mathis, P., & Oesterhelt, D. (1993) *Biochemistry 32*, 10894−10904.
Williams, J. C., Alden, R. G., Murchison, H. A., Peloquin, J. M., Woodbury, N. W., & Allen, J. P. (1992) *Biochemistry 31*, 11029−11037.
Zinth, W., Arlt, T., Penzkofer, H., Hamm, P., Dohse, B., & Oesterhelt, D. (1995) in *Photosynthesis: from Light to Biospere* (Mathis, P., Ed.) Vol. I, pp 389−394, Kluwer Academic Publishers, Dordrecht, The Netherlands.

BI960185F